

*Dedicated to Prof. Dorin N. Poenaru's  
70th Anniversary*

## RECENT APPLICATIONS OF SELF-CONSISTENT MEAN-FIELD MODELS

T.J. Bürvenich

*Frankfurt Institute for Advanced Studies, J.W. Goethe University  
Max-von-Laue-Str. 1, D-60438 Frankfurt am Main, Germany  
E-mail: buervenich@fias.uni-frankfurt.de*

(Received February 23, 2007)

*Abstract.* The framework of self-consistent models and their predictive power for known nuclei are discussed. Recent applications to clustering in light nuclei, superheavy nuclei as well as to laser-nuclear physics are reviewed.

*Key words:* self-consistent mean-field models, superheavy nuclei, clusters, laser-nuclear physics.

### 1. INTRODUCTION

Throughout the years nuclear structure physics has revealed interesting phenomena related to nuclear ground-state properties and excitations such as octupole deformations in the ground state, triaxial deformations, the phenomena of neutron skins and halos, Boromean systems, exotic excitations like Pygmy resonances and many more. The theoretical description of a nucleus deals with two regimes in which approximations have to be made. Firstly, since we are dealing with a many-body system, we need to introduce many-body approximations. Secondly, the in-medium nucleon-nucleon interaction needs to be parametrized and cannot (yet) be deduced from QCD. This is different in atomic physics, for example, where the interaction mediated by photons is known to a very high degree<sup>1</sup> and the main approximations are dealing with the many-body aspect. Moreover, nuclei are self-organized systems and do not possess an external potential as, for example, atoms. These properties of

---

<sup>1</sup> Quantum Electrodynamics delivers most precise predictions and yet no discrepancy with experiment has been found.

the nucleus make nuclear physics both exciting and extremely difficult. They are also the reason for the many different nuclear models that have been built throughout the decades: the simple liquid-drop formula, the phenomenological shell model, the macroscopic-microscopic method, self-consistent mean-field models, Greensfunction-Monte-Carlo, shell model and no-core shell model, and many others. In this contribution, self-consistent mean-field models will be discussed and illustrated with a few typical applications.

## 2. FRAMEWORK

The ansatz of self-consistent mean-field models (for a comprehensive review see Ref. [1]) is traditionally based on the parametrization of the effective nucleon-nucleon interaction between point-like nucleons. The modern way is the construction of the energy functional which can incorporate terms that can not be formulated in terms of effective interactions.

The relativistic mean-field (RMF) model can be formulated in terms of a Lagrangian employing the relevant degrees of freedom which are nucleon and the boson fields:

$$\mathcal{L} = \mathcal{L}_{\text{nucleon}}^{\text{free}} + \mathcal{L}_{\text{meson}}^{\text{free}} + \mathcal{L}_{\text{coupl}}^{\text{lin}} + \mathcal{L}_{\text{coupl}}^{\text{nonlin}}. \quad (1)$$

The first parts are Lagrangians for free nucleons and mesons and the photon:

$$\mathcal{L}_{\text{nucleon}}^{\text{free}} = \hat{\psi}(i\gamma_{\mu}\partial^{\mu} - m)\hat{\psi}, \quad (2)$$

$$\begin{aligned} \mathcal{L}_{\text{meson}}^{\text{free}} = & \frac{1}{2}(\partial_{\mu}\hat{\sigma}\partial^{\mu}\hat{\sigma} - m_{\sigma}^2\hat{\sigma}^2) - \frac{1}{2}\left(\frac{1}{2}\hat{G}_{\mu\nu}\hat{G}^{\mu\nu} - m_{\omega}^2\hat{\omega}_{\mu}\hat{\omega}^{\mu}\right) \\ & - \frac{1}{2}\left(\frac{1}{2}\hat{B}_{\mu\nu} \cdot \hat{B}^{\mu\nu} - m_{\rho}^2\hat{\rho}_{\mu} \cdot \hat{\rho}^{\mu}\right) - \frac{1}{4}\hat{F}_{\mu\nu}\hat{F}^{\mu\nu}. \end{aligned} \quad (3)$$

It is worth mentioning that these meson fields have only loose correspondence with the physical meson spectrum. Mean-field models employing contact interactions between nucleons have a comparable predictive power for nuclear ground-state observables and excited states [2, 3, 4].

A theory of interacting fields is achieved by introducing minimal couplings between the mesons/photon and the nucleonic densities and currents.

$$\mathcal{L}_{\text{coupl}}^{\text{lin}} = -g_{\sigma}\hat{\sigma}\hat{\psi}\hat{\psi} - g_{\omega}\hat{\omega}_{\mu}\hat{\psi}\gamma^{\mu}\hat{\psi} - g_{\rho}\hat{\rho}_{\mu} \cdot \hat{\psi}\vec{\tau}\gamma^{\mu}\hat{\psi} - e\hat{A}_{\mu}\hat{\psi}\frac{1+\tau_3}{2}\gamma^{\mu}\hat{\psi}. \quad (4)$$

The density dependence of the scalar field needs to be altered to reproduce the compressibility of nuclear matter and to obtain a quantitative description of nuclei:

$$\mathcal{L}_{\text{coupl}}^{\text{nonlin}} = \frac{1}{2}m_{\sigma}^2\hat{\sigma}^2 - U_{\sigma}[\hat{\sigma}]. \quad (5)$$

This is often done by an expansion in powers of the field. The field tensors of the mesons are written down in direct analogy to the electromagnetic field tensor.

Each term in the Lagrangian introduces a coupling constant that needs to be adjusted which will be discussed later in this section. The equations of motion can be obtained in the standard fashion by the Euler-Lagrange equations. This model is free of assumptions on the nuclear potential or density distributions which are the outcome of a (converged) calculation. Self consistency can produce effects such as density depletion in superheavy nuclei which are less likely to occur in other approaches.

The binding properties of nuclear matter and nuclei are generated from the strong scalar and vector fields,  $V_S = g_\sigma \sigma \approx -350$  MeV,  $V_V = g_\omega \omega^0 \approx +300$  MeV, adding up to  $V = V_S + V_V \approx -50$  MeV. They add up with the same sign to generate the strong spin-orbit potential in nuclei, which is given by

$$V_{ls} \propto \frac{d}{dr}(V_S - V_V \gamma_0) \vec{l} \cdot \vec{s}. \quad (6)$$

This spin-orbit force emerges from the covariant formalism with right sign and magnitude without introducing additional parameters. This is where relativity shows up most clearly in these covariant models – the dynamics of the nucleons on the contrary justifies the use of non-relativistic models.

Self-consistent models for the nucleus have recently experienced a reinterpretation in terms of *effective field theory* and *density functional theory* [5], which partly explains their success in accurately describing nuclear ground-state properties. As effective field theories for nucleonic degrees of freedom, they are constructed to incorporate explicitly physics below a certain energy scale  $\lambda$ , which is of  $\mathcal{O}$  (1 GeV). Short-distance physics and correlations, vacuum polarization and all effects at higher energies are being absorbed into the various interaction terms and coupling constants.

The *Hohenberg-Kohn theorem* [6, 7] states that the energy of a many-body state is a unique functional of its density. Thus, *in principle*, it is possible to achieve an exact treatment of such a system if the right energy functional is found. In such a description, all correlations are present in the energy and the density distribution (not in the wave-function, however, which is a Slater-determinant of Kohn-Sham orbitals). For the description of a self-bound nuclear system in the intrinsic frame, generalizations of this theorem are necessary and available [8]. Unfortunately, these theorems are non-constructive and provide no handle for the development of such functionals. Thus, current efforts involve ways to systematically construct these functionals and subsequently improve them. As mentioned before, each term introduced in the ansatz of the model is associated with a free parameter. These parameters

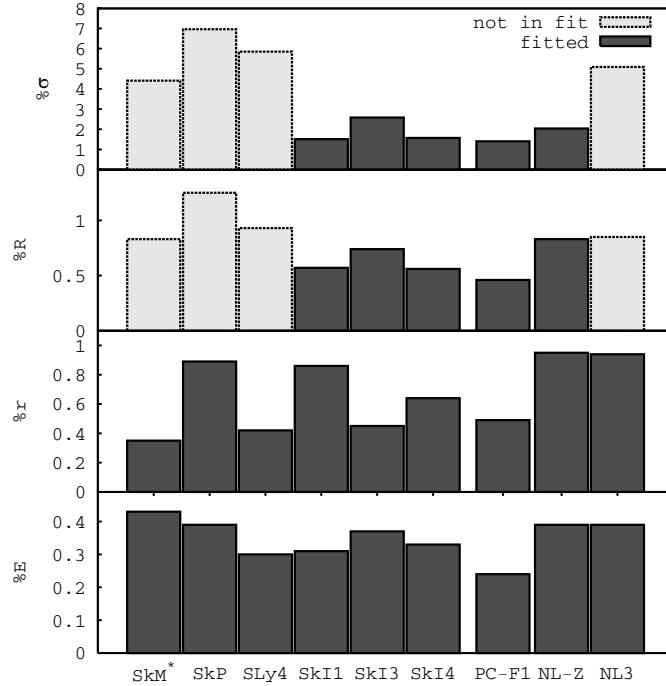


Fig. 1 – Errors in percent for the mean-field forces as indicated and the observables (from top to bottom) surface thickness, diffraction radius, rms radius, and binding energy. Dark columns indicate that this observable has not been fitted, light columns indicate observables which have been part of the adjustment procedure.

(between 6 and 12) are being fitted to experimental data of nuclear ground-state properties. It is interesting to assess the quality of various forces with different adjustment procedures for various observables. Fig. 1 summarizes such a comparison for various Skyrme forces (SkM\*, SkP, SLy4, SkI1, SkI3, SkI4), a point-coupling RMF force (PC-F1) and two standard RMF forces (NL-Z and NL3). Shown is the error in percent for the observables (from top to bottom) surface thickness, diffraction radius, rms radius, and binding energy. These errors have been averaged over a selection of nuclei throughout the nuclear chart. Starting with the binding energy, this observable is always part of the adjustment procedure, and the quality of modern models can describe it with an accuracy below 0.5%. The rms radius as the prominent information about the nuclear density distribution is usually taken into account in the adjustment, and its mean error lies below 1%. The other two form-factor-related observables, diffraction radius and surface thickness, are in some cases not taken into account in the adjustment. As can be inferred from the figure, its inclusion in the adjustment procedure can lead to a slightly better description.

The biggest effect, however, is seen for the surface thickness. Firstly, the error scale is larger and ranges within several percent error. Secondly, an inclusion of this observable in the adjustment procedure can considerably decrease its error. Self-consistent mean-field models tend to underestimate the size of the surface thickness. This can be attributed to missing correlations and/or the missing long-range (pion) dynamics.

### 3. NUCLEAR MOLECULAR STATES

The existence of nuclear molecules was discovered [9] in experiments on the resonances observed in excitation functions of elastic and inelastic scattering of  $^{12}\text{C}$  on  $^{12}\text{C}$  [10, 11] In this section, we report on some examples for the occurrence of clustering in light nuclei within the RMF model [12].

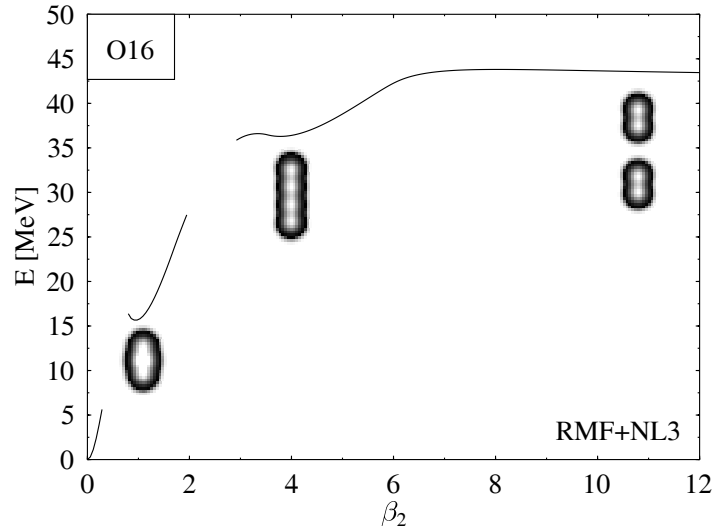


Fig. 2 – Reflection-symmetric and axialsymmetric PES of  $^{16}\text{O}$ . Parts where the calculation does not converge are left out.

In order to detect clustering for ground and excited states, we compute the energy of the system as a function of deformation. The cuts through the potential energy surface (PES) are calculated in axial symmetry for reflection-symmetric and -asymmetric shapes using a constraint on the total quadrupole moment  $Q_{20}$  of the nucleus. This is achieved by adding  $-\lambda \hat{Q}_{20}$  to the Hamilton operator and minimizing  $\langle \hat{H} - \lambda \hat{Q}_{20} \rangle$ . All other multipole moments that are allowed by the symmetry of the calculation are not constrained and adjust themselves corresponding to the solution of minimal energy. So, in contrast to

the macroscopic-microscopic approach [13], we are not operating in a limited deformation space. On the other hand, we are not necessarily exactly following the gradient in the multidimensional PES which would only be the case if the fission valley would be parallel to the  $Q_{20}$  direction [14].

The energy of the system is minimized using the damped gradient iteration method [15]. The mean-field equations are solved in coordinate space employing derivatives as matrix multiplications in Fourier space. We do not correct spurious rotational or vibrational motion, corresponding to zero-point energies which would lower the total energy and modify the structure of the PES.

As the first system, we consider  $^{16}\text{O}$ . Its potential energy surface can be seen in Fig. 2. The PES reveals two local minima corresponding to two isomeric states with a cluster configuration. At  $\beta_2 = 0.97$ , at an energy of about 15 MeV above the ground-state energy, a  $\alpha$ - $^8\text{Be}$ - $\alpha$  configuration is found. The  $^8\text{Be}$  nucleus is, however, not in its groundstate. At  $\beta_2 = 3.78$ , a local minimum in the PES corresponds to a chain of 4  $\alpha$ -particles at an energy of around 36 MeV. The following PES at larger deformations corresponds to symmetric fission of oxygen into two  $^8\text{Be}$  nuclei. In each fragment, a double- $\alpha$ -structure is clearly visible.

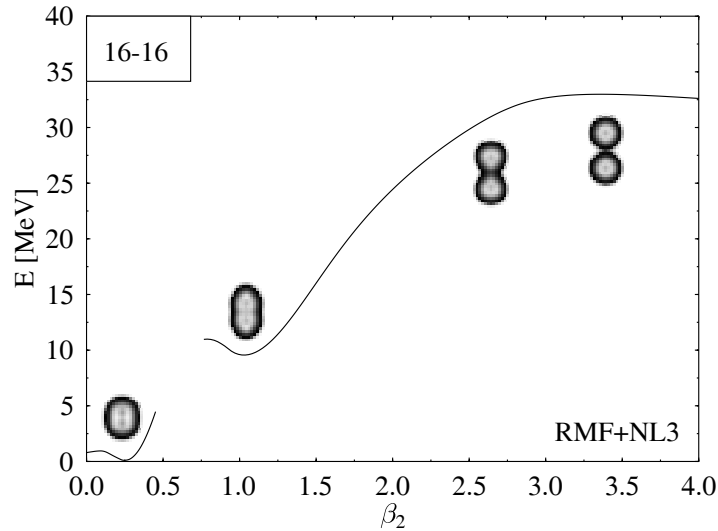


Fig. 3 – Reflection-symmetric and axialsymmetric PES of  $^{32}\text{S}$ . Parts where the calculation does not converge are left out.

Another interesting system is  $^{32}\text{S}$  corresponding to two times  $^{16}\text{O}$ . The reflection-symmetric PES can be seen in Fig. 3. The system has a deformed ground state at  $\beta_2 = 0.27$ . Its density distribution corresponds to a twofold structure with lowered density in the middle of the two halves. At  $\beta_2 = 1.04$ ,

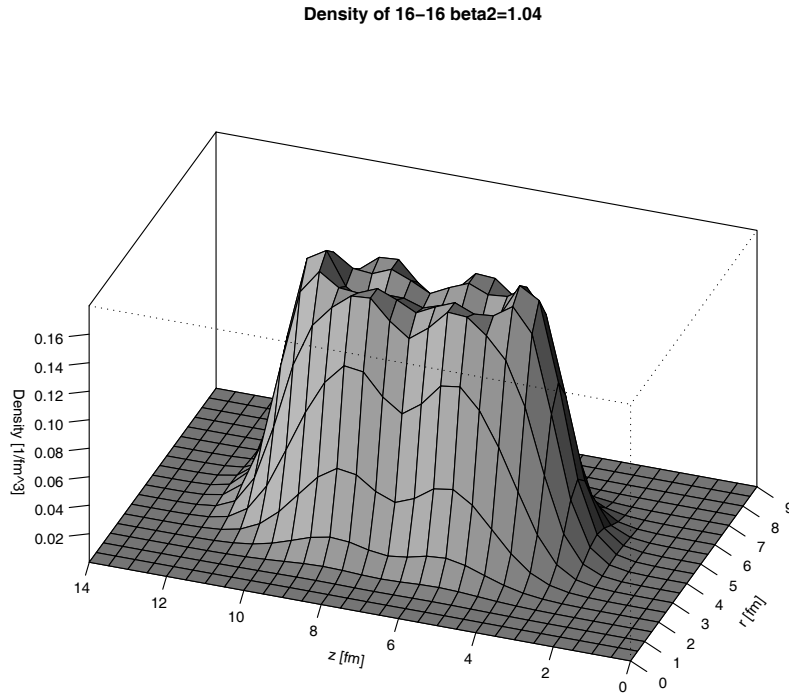


Fig. 4 – Baryon Density of  $^{32}\text{S}$  at  $\beta_2 = 1.04$ .

a second local minimum occurs. The density distribution exhibits a cluster structure corresponding to two  $^{16}\text{O}$  nuclei, though no pronounced neck between the fragments has built (see also Fig. 4). For larger deformations, a neck develops and the systems fission symmetrically. The isomeric state found here can be associated with a two- $^{16}\text{O}$ -cluster state.

Investigations of these and similar systems in the framework of the Skyrme-Hartree-Fock approach can be found in Ref. [16].

#### 4. SUPERHEAVY NUCLEI

Superheavy nuclei are nuclei with proton numbers above  $Z \approx 110$ . These systems owe their stability only to quantum-mechanical shell effects. The liquid-drop description predicts no stable ground state. While the nucleon-nucleon interaction is short-range and saturating, the Coulomb force, even though it is much weaker, has long-range nature. Thus, while a proton can only interact with its neighbors through the nuclear force, it feels all surrounding protons. Due to shell effects, however, the system can gain stability, and

spontaneous fission proceeds through the fission barrier. For these systems, alpha decay and spontaneous fission become competing decay modes. While superheavy nuclei can on earth be only produced in experiments with heavy ions, they might come to existence in the universe in processes such as supernova explosions. With respect to the testing of nuclear models, superheavy nuclei act as magnifying glasses for nuclear structure effects that are present but less visible in nuclei closer to stability.

In the following, we will examine the stability of a selection of superheavy nuclei with respect to spontaneous fission. We will first discuss spontaneous fission in actinide nuclei. A typical fission barrier is shown in Fig. 5. The nucleus  $^{252}\text{Cf}$  possesses a symmetric fission barrier and the asymmetric solution, which is energetically favorable. At a deformation of  $\beta_2 = 1.0$ , an isomeric state of approximately the same energy as the ground state is present. The figure furthermore displays symmetric and asymmetric solutions for separated fragments which intersect the branches of the elongated nuclear system with a neck. These various branches are separated from each other by small barriers in the multi-dimensional potential energy surface. It is a present challenge to obtain smooth fission and fusion barriers within these approaches.

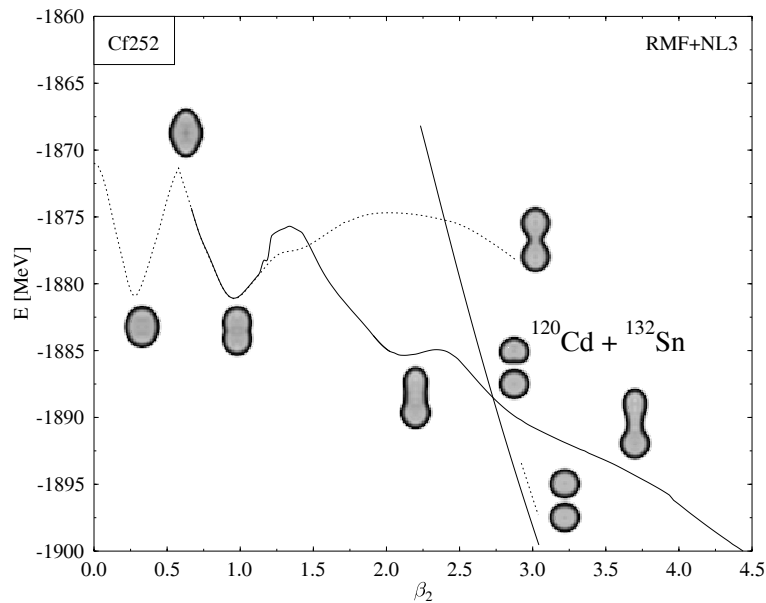


Fig. 5 – Symmetric fission barrier (dashed line), asymmetric fission barrier (full line) and solutions for two separate fragments with combinations as indicated.

The systematics of fission barriers for superheavy nuclei ranging between  $Z = 108 - 120$  is shown in Fig. 6 [17]. The symmetric barriers are shown with

full lines, the asymmetric barriers (allowing reflection-asymmetric shapes) are shown with a dashed line. Note that the first barrier is always reflection-symmetric. Going up in  $Z$  and  $N$  we find a transition from well-deformed nuclei via transitional nuclei displaying shape isomerism to spherical nuclei at the upper right end of the chart. The barriers in the transitional region become rather small. The inclusion of asymmetry makes the second (symmetric) barrier vanish for  $Z \geq 114$ , thus these superheavy systems only have one single barrier to tunnel through. This is an important difference to the case of actinide nuclei which usually possess two barriers.

The same barriers, calculated with Skyrme forces, show the same general trends, but exceed the RMF barriers for high charge numbers considerably. A similar situation occurs already for actinide nuclei: while RMF produces rather low and sometimes too low barriers, SHF tends to larger barriers [17].

These different predictions are rather model dependent than force dependent<sup>2</sup> The reason for these differences is related to the different macroscopic and shell-structure-related properties of the various forces. For example, while the RMF forces predict the magic numbers at  $Z = 120$  and  $N = 172, 184$ , SHF forces place them at  $Z = 114, 120, 126$  and  $N = 184$ . Moreover, the asymmetry energy of standard RMF forces with  $a_4 \approx 38$  MeV is too large compared to the empirical value of  $a_4 \approx 30 - 34$  MeV. Skyrme forces perform better at reproducing this result. The search for the underlying model properties that lead to these different predictions is still ongoing. This situation, however, indicates that at the present stage reliable predictions for the fission barriers of superheavy elements, and their corresponding life times, cannot be made.

## 5. LASER-NUCLEAR PHYSICS

Present and near-future laser facilities will provide a gateway to direct (electromagnetic) laser-nucleus interactions. Nuclear quantum optics involving x-ray laser facilities will soon demonstrate direct laser-nucleus interactions [18]. An application involving strong laser fields in the optical regime is the dynamic (AC) Stark shift of proton states in atomic nuclei. Similarly to the case of a constant electric field, in an oscillating laser field applied to an atom (nucleus) the electron (proton) levels experiences a small shift. These shifts may serve as a signal for direct laser-nucleus interactions.

An increase of the laser frequency and field strength can be achieved by head-on collisions of the nuclei and the laser pulses. In the rest frame of the nucleus, the Doppler shifted electric field strength  $E_N$  and the frequency  $\nu_N$

---

<sup>2</sup> This is true if the adjustment protocols of the forces do not differ dramatically.

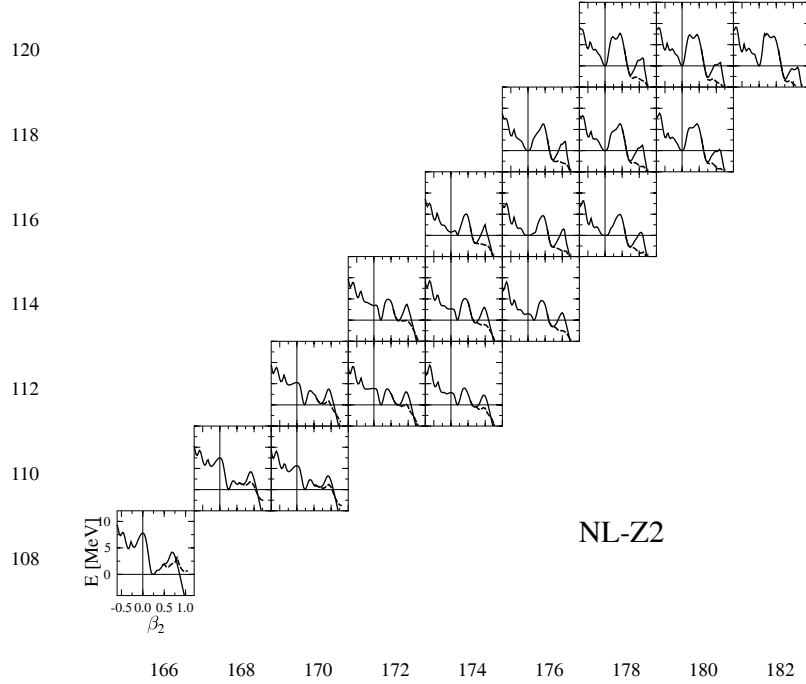


Fig. 6 – Reflection-symmetric (full line) and reflection-asymmetric (dotted line) fission barriers calculated with the RMF force NL-Z2.

are given by

$$E_N = \sqrt{\frac{1+\beta}{1-\beta}} E_L = (1+\beta)\gamma E_L, \quad (7)$$

$$\nu_N = \sqrt{\frac{1+\beta}{1-\beta}} \nu_L = (1+\beta)\gamma \nu_L, \quad (8)$$

where subscript  $N$  denotes the nuclear rest frame and  $L$  the laboratory frame, respectively. The laser-nucleus interaction is treated in the electric dipole approximation, in which the (non-relativistic) interaction term in the length gauge is given by [19, 20]

$$H_I = -e\vec{E}(t) \cdot \vec{r}. \quad (9)$$

Here,  $e = |e|$  is the electron charge,  $\vec{E}(t)$  is the electric field, and  $\vec{r}$  the position operator. For light linearly polarized in  $z$ -direction, this reduces to  $H_I = -eE(t)z$ . The total Hamiltonian of our system is thus

$$H = H_0 + H_I, \quad (10)$$

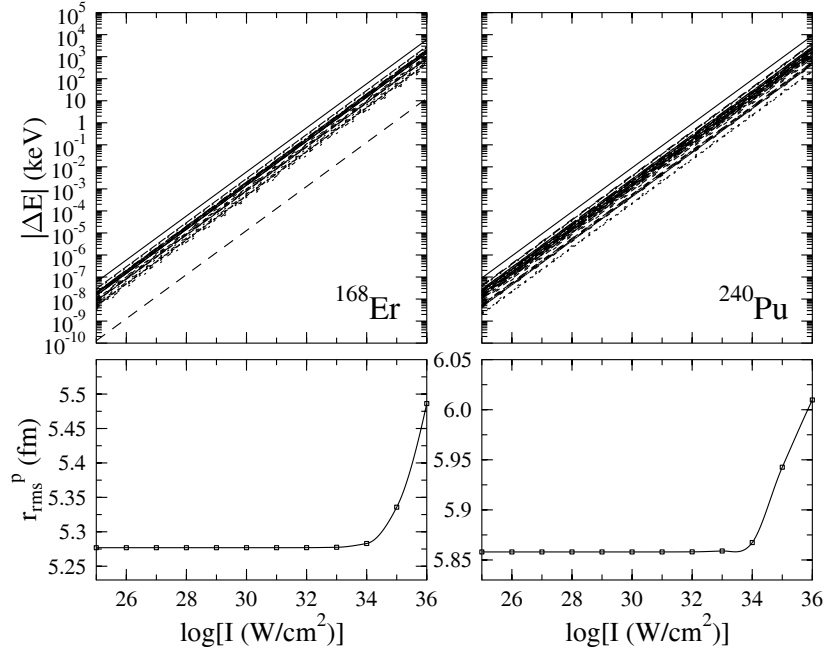


Fig. 7 – AC-Stark shifts of the proton single-particle states in the laser field (upper row, displayed on a  $\log_{10}$  scale) as a function of laser intensity in the nuclear rest frame for the nuclei as indicated, and proton rms radii (lower row) as a function of laser intensity in the nuclear rest frame. Each line in the upper figures corresponds to a Stark shift of a proton single-particle level. The widths of these bands characterize the spread in these shifts. In the lower figure, the square dots indicate the calculated results, which for convenience are connected by the thin line.

where  $H_0$  denotes the nuclear Hamilton operator that is specified by the nuclear model employed and has been described in Section 2.

A few comments on the choice of this interaction are in order. The spatial dependence of the electric laser field is neglected in the dipole approximation due to the small extension of the nucleus of the order of a few femtometers. The magnetic fields can also be neglected due to the smallness of the laser-nucleus interaction. Here we have an important difference to atomic systems: intensities considered large on atomic scales (they compete with the Coulomb force of the nucleus), typically are still weak as compared to the much stronger force between nucleons. Hence a non-relativistic treatment is justified in our case. The nuclear model employed in this study provides a covariant framework for the nuclear ground-state description. Note, however, that the nucleons within the nucleus move non-relativistically. The predominant relativistic

feature is the strong spin-orbit force in nuclei, which is an intrinsic ingredient in a covariant description employing strong scalar and vector fields.

The Stark shifts of the single-proton states  $|n\rangle$  are given by

$$\Delta E_n = \frac{1}{2} \sum_{m \neq n} \frac{\langle n | H_I | m \rangle \langle m | H_I | n \rangle}{\epsilon_n - \epsilon_m}. \quad (11)$$

The states  $|n\rangle$  are taken from the relativistic mean-field calculation, and the matrix elements of the dipole operator sandwiched between two states are calculated numerically.

The proton rms radius is defined as [21]

$$r_{rms}^p = \sqrt{\frac{\int d^3x r^2 \rho^p(\vec{x})}{\int d^3x \rho^p(\vec{x})}}, \quad (12)$$

with  $r = \sqrt{x^2 + y^2 + z^2}$ ,  $\rho^p(\vec{x})$  is the proton point density. Note that this definition also holds for non-spherical density distributions. The rms radius is related to the spatial extension of the density distribution. The experimentally accessible quantity in nuclei is the nuclear charge radius which can be extracted from the corresponding measured form factor.

The AC Stark shifts of single proton states in the nuclei  $^{168}\text{Er}$  and  $^{240}\text{Pu}$ , as well as the corresponding rms proton radii are displayed in Fig. 7. We have chosen these nuclei as typical representatives of intermediate and heavy nuclei. Their lowest measured E1 excitations lie at 1.359 MeV ( $^{168}\text{Er}$ ) and 0.555 MeV ( $^{240}\text{Pu}$ ), respectively [22]. Thus, transitions will not be excited by the considered laser energies of  $\mathcal{O}(\text{keV})$  in the nuclear rest frame. Lower excitations of even parity would require two- or higher-order photon processes, and their energies are still more than 20 keV above the ground-state energy. Thus the Stark effect can be treated separately from nuclear excitation mechanisms.

Shifts of  $\approx 1$  keV are reached at intensities of roughly  $10^{32}$  W/cm<sup>2</sup> for the systems discussed here (intensities of  $10^{34}$  W/cm<sup>2</sup> are necessary for lighter systems such as oxygen). These shifts are approximately a factor of 10 – 1 000 smaller than typical energy differences of single-particle levels close to the Fermi edge. As expected, in absolute terms, they are much larger than shifts appearing in atomic systems, but may also surpass them in relative terms. The size of the shifts depends both on the matrix elements  $\langle m | H_I | n \rangle$  as well as on the number of states contributing with dipole moments and their corresponding single-particle energies.

## 6. OUTLOOK

Self-consistent mean-field models have reached a high predictive power for the description of nuclear ground-state observables. Furthermore, they can be applied to excited states, a topic that has not been touched in this contribution. Their application can increase our understanding of phenomena like nuclear clustering, superheavy nuclei, and even the interplay of laser fields with nuclei. As was discussed, their predictions for fission barriers allow no quantitative conclusions at this stage, since the uncertainties displayed by a selection of models are too large. Thus, further improvements of these approaches are mandatory in the near future.

*Acknowledgements.* The author would like to acknowledge interesting and fruitful discussions with D. Poenaru, and wishes him all the best for the forthcoming years.

## REFERENCES

1. M. Bender, P.-H. Heenen, P.-G. Reinhard, *Rev. Mod. Phys.*, **75**, 121 (2003).
2. B.A. Nikolaus, T. Hoch, and D.G. Madland, *Phys. Rev.*, C **46**, 1757 (1992).
3. T. Bürvenich, D.G. Madland, J.A. Maruhn, and P.-G. Reinhard, *Phys. Rev.*, C **65**, 044308 (2002).
4. T. Niksic, D. Vretenar, and P. Ring, *Phys. Rev.*, C **72**, 014312 (2005).
5. R.J. Furnstahl, *Lect. Notes Phys.*, **641**, 1-29 (2004).
6. W. Hohenberg and L.J. Sham, *Phys. Rev.*, A **140**, 1133 (1965).
7. R.M. Dreizler and E.K.U. Gross, *Density Functional Theory*, Springer, 1990.
8. J. Engel, *nucl-th/0610043*.
9. D.A. Bromley, J.A. Kuehner and E. Almqvist, *Phys. Rev. Lett.*, **4**, 365 (1960).
10. W. Greiner, J.Y. Park and W. Scheid, *Nuclear Molecules*, World Scientific, Singapore, 1994.
11. W. Greiner and D.N. Poenaru, *Rom. Rep. Phys.*, **44**, 713 (1992).
12. T. Bürvenich and D.N. Poenaru, Report WP18 IDRANAP 30-02/2002.
13. P. Möller, J.R. Nix, W.D. Myers, and W.J. Swyatecki, *At. Data Nucl. Data Tables*, **59**, 185 (1995).
14. H. Flocard, P. Quentin, A.K. Kerman and D. Vautherin, *Nucl. Phys.*, **A203**, 433 (1973).
15. P.-G. Reinhard and R.Y. Cusson, *Nucl. Phys.*, **A 378**, 418 (1982).
16. J.A. Maruhn, M. Kimura, S. Schramm, P.-G. Reinhard, H. Horiuchi, A. Tohsaki, *Phys. Rev.*, C **74**, 044311 (2006).
17. T. Bürvenich, M. Bender, J.A. Maruhn, P.-G. Reinhard, *Phys. Rev.*, C **69**, 014307 (2004); Erratum-ibid., C **69**, 029901 (2004).
18. T.J. Bürvenich, J. Evers, and C. H. Keitel, *Phys. Rev. Lett.*, **96**, 142501 (2006).
19. M. Sargent III, M.O. Scully, and W.E. Lamb Jr., *Laser Physics*, Westview Press, 1993.
20. J.M. Eisenberg and W. Greiner, *Nuclear Theory*, Volume 2: "Excitation Mechanisms of the Nucleus", North-Holland, 1970.
21. P. Ring, P. Schuck, *The Nuclear Many-Body Problem*, 2nd printing, Springer, 2000.
22. \* \* \*, LBNL Isotopes Project, <http://ie.lbl.gov/toi.html>.